GLAD: the IPNS Glass, Liquid, and Amorphous Materials Diffractometer

R. K. Crawford, D. L. Price, J. R. Haumann, R. Kleb, D. G. Montague, J. M. Carpenter, S. Susman and R. J. Dejus
Argonne National Laboratory
Argonne, IL
USA

Introduction

A number of years of experience in diffraction from amorphous materials has now been accumulated at various pulsed neutron sources. Workshops at IPNS and elsewhere have distilled some of this experience to provide a set of criteria for a new diffractometer dedicated to and optimized for structural studies of amorphous materials. These criteria include:

1. All Q values should be measured with as short wavelengths and small scattering angles as possible to minimize both inelasticity and attenuation corrections for highly absorbing samples. The workshops suggested that a wavelength range of ~0.2 - 2 Å would be appropriate. A large solid-angle detector at small scattering angles is required to make an efficient instrument under these conditions.

2. Wavelength and angle information should be kept separate (no time-focusing) until wavelength-dependent corrections have been made.

3. The instrument should provide a high incident flux and a large scattered solid-angle coverage so that reasonable data rates can be achieved with small samples and a rapid turnaround time is possible with larger samples.

4. Resolution should be adequate for the problems but no greater than necessary to keep the data rates as high as possible. The workshops suggested that resolutions ranging from $\Delta Q = 0.005$ Å^{-1} at $Q = 0.05$ Å^{-1} to $\Delta Q = 0.15$ Å^{-1} at $Q = 20$ Å^{-1} would be appropriate. The implications of these resolution requirements are discussed further below.

This paper discusses the instrument GLAD (Glass, Liquid, and Amorphous Materials Diffractometer) which has been designed to meet these criteria and is now being built at IPNS. This instrument involves the use of relatively short-wavelength neutrons and a sophisticated neutron detection and acquisition system. A preliminary, simplified version of the instrument has been constructed while the final version is still under design, in order to develop the data acquisition and analysis techniques and to develop methods for collection of data with adequate quality (low background) at short wavelengths. This paper will briefly outline the final instrument envisioned and its calculated performance, but will focus mostly on the details of the detection/acquisition system and the calibration and data collection procedures which have been developed. The brief operating experience which has been gained to date with the preliminary instrument version will also be summarized.

Conceptual Design and Projected Performance

The design criteria noted above have led directly to several features of GLAD. In particular, the incident flight path should be short to provide high intensities. Angular considerations rather than wavelength uncertainties dominate the resolution at the small scattering angles of interest here, so the incident path can be as short as is permitted by the space constraints at IPNS. Soller collimators can be used to provide the necessary angular resolution for the incident beam, so a relatively large sample size and the full moderator size can be utilized with no loss in resolution.

Figure 1 shows a sketch of the final version of GLAD as currently conceived. This instrument will have a 9.0 m incident flight path (the minimum value consistent with spatial constraints on the beamline chosen at IPNS), and a 3.0 m "diameter" scattered flight path. Two sample positions are provided. The 9-meter "high-resolution" position is located where the beam enters the scattered flight path, and the "high-intensity" position is located 1.5 m further downstream at the center of the scattered flight path. Converging soller collimators, focused at the point where the beam exits the scattered flight path (3.0 m from the high-resolution sample position), provide incident beam collimation of 0.007 rad FWHM in the horizontal and vertical directions. The circular detector locus then eliminates the sample size as a factor in the resolution when the sample is located at the high resolution position.[1] At the high-intensity position this focusing is still effective for small scattering angles, but is ineffective at the higher scattering angles. However, using this sample position places the sample much closer to the detectors and hence provides a much greater solid angle for detection of the scattered neutrons - thus the name "high-intensity". As shown in the figure, the detector positions

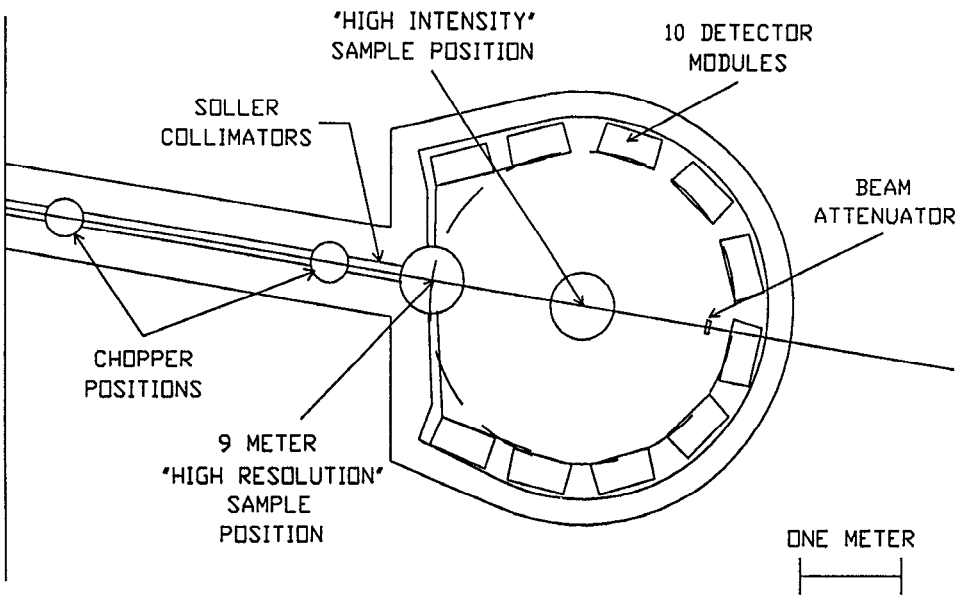

Fig. 1 Plan view of the GLAD instrument.

nearest the high-resolution sample position deviate somewhat from the circular locus, reducing the detector size contributions to the resolution to acceptable values.

With this flight path configuration the desired resolution can be achieved (for the high-resolution position) by using detectors which are ~ 1 cm in diameter. At small scattering angles the spatial resolution along the axes of the detectors must be of comparable magnitude, so position-sensitive detectors must be used. Two-dimensional proportional counters suffer from data rate limitations, so we have chosen to use cylindrical linear position-sensitive detectors (PSD). The position encoding scheme used for these detectors is discussed below. The detectors are located in a controlled atmosphere, outside the scattered-flight-path vacuum and separated from the vacuum by thin Al windows. The detectors are mounted with their axes normal to and centered on the scattering plane, in "modules" which each contain ~ 40-60 detectors and a mechanism for providing absolute position calibration. This position-calibration mechanism consists of a neutron-absorbing bar which can be driven to various known positions in front of the detectors by a stepping-motor system. Individual detector positions within each module are chosen to provide as nearly continuous angular coverage as possible while preventing "shadowing" by adjacent detectors when either sample position is used. As shown in Fig. 1, the locations of the detector modules are not symmetrical about the incident

beam, so that detectors on one side will cover the gaps in angular range on the other side necessitated by the flight path structural components and detector calibration mechanisms. Figure 2 shows a typical mounting arrangement for the detectors, preamplifiers, and detector calibration mechanism in one detector module. A beam "attenuator" upstream from the flight path exit window absorbs most of the direct beam before it reaches the detectors, allowing the PSD bank to operate in the forward-scattering direction.

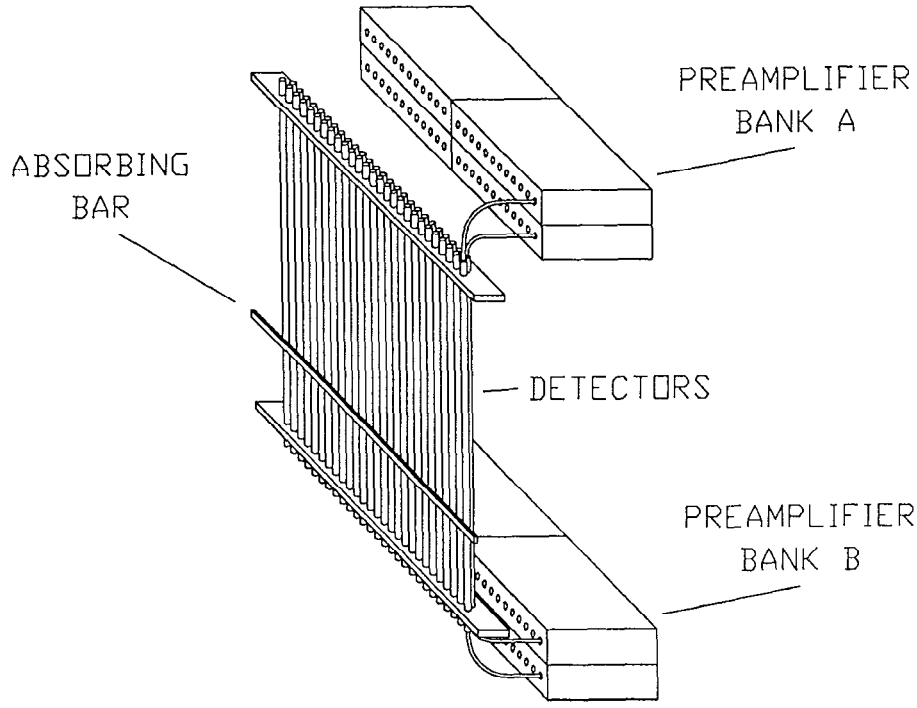

Fig. 2 Schematic representation of the detector module intended for the forward scattering direction, showing detectors, preamplifiers, and the absorbing bar for position calibration. Modules for other scattering angles are similar, although detector shadowing considerations lead to location of detectors in a single row, rather than the staggered double row shown here, for most of the higher-angle modules. For clarity, only two of the sets of coaxial cables between the detectors and preamplifiers are shown, and the drive mechanism for the absorbing bar is omitted from the drawing.

The scattered flight path will be evacuated, and in cases where sample environment is not of particular importance, samples can be mounted directly in the flight path vacuum with no other windows to contribute to the scattering. When sample environment must be controlled, as for cryostats or furnaces, a thin-windowed "well" can be used to separate the sample environment from the flight path vacuum.

As can be seen in Fig. 1, the incident beamline includes provisions for the installation of Fermi choppers when desired. Since the use of a chopper will drastically reduce the overall data rate, this is not expected to be the normal operating mode. However this capability will allow the collection of elastic-scattering rather than total-scattering data when required for specific problems. It is also possible that a second, somewhat different chopper may be needed in the incident beam to suppress background originating from the prompt pulse or from scattering in the main chopper, so two different chopper locations have been provided.

Figure 3 shows the calculated performance for this instrument. These data are based on Monte Carlo simulations which trace neutron paths from the moderator, through the collimators and sample, and into the detectors. The results presented here include effects of the Soller collimators. The simulations predict values of resolution which are nearly equal for each detector position-element with the same Q-value, independent of the scattering angle and the vertical position on the detector. The resolution $\Delta Q/Q$ shown in Fig. 3 is in line with the resolution goals stated above. For low values of Q, $\Delta Q/Q$ increases rapidly as Q decreases, while it reaches a nearly constant value slightly larger than 1% for Q greater than 5 $Å^{-1}$. These results were calculated by summing, with equal weight, all detector elements contributing to the same range of Q. The resolution for the individual detector elements is somewhat better, but since the angular coverage for each element is slightly different, the summing process degrades the resolution. Estimates of count rate are based on measurements done on the Special Purpose Powder Diffractometer (SEPD) at IPNS. This estimate of intensity is the sum of all elements with the same average Q-value, assuming ~ 450 detectors in the 10 modules as shown, and corresponds to the composite resolution $\Delta Q/Q$ shown in the lower curve in Fig. 3.

Temporary Flightpath

Because of the long lead time required for design and procurement of the vacuum flight path for this instrument, it was decided to begin with a temporary flight path while the final unit is still under design. This will

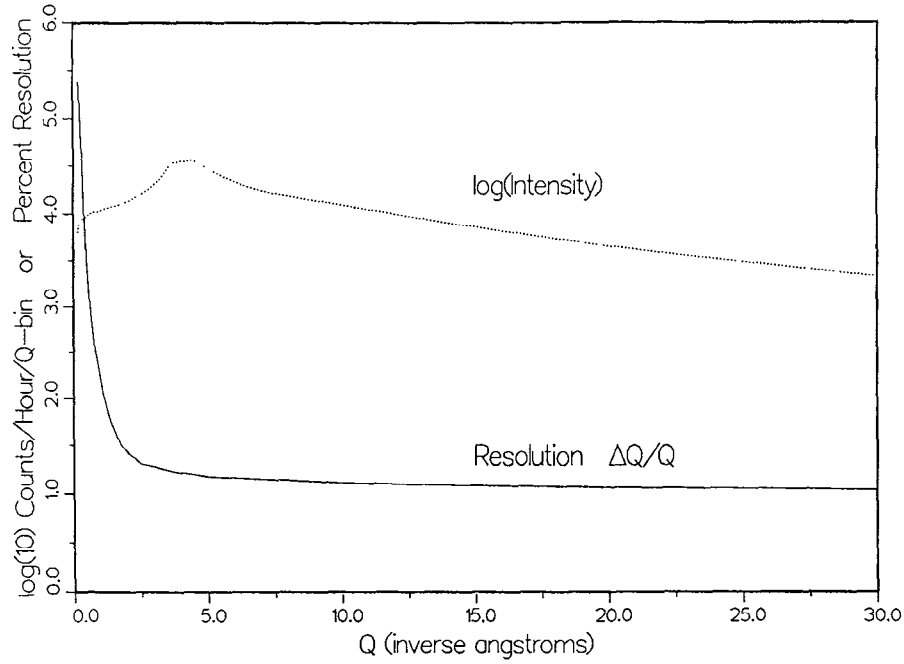

Fig. 3 Calculated resolution (FWHM) and intensity for GLAD. The calculated values are based on a 1 cm square x 1 mm thick vanadium sample at the high-resolution sample position, and are for an instrument geometry and detector locations approximately as shown in Fig. 1.

enable us to gain experience in the use of the rather complicated detector/data-acquisition system envisioned, to begin work on reducing the backgrounds at short wavelengths, and to develop methods for handling and analyzing data sets of the expected magnitude (see below for projections). The temporary flight path is shown schematically in Fig 4. This path allows the use of one complete detector module with 55 detectors, as shown in Fig. 2, providing scattering angles up to ± 9°. An evacuable chamber is provided so that samples can be in cryogenic or other environments, but the scattered flight path is Ar-filled rather than evacuated. To increase intensities, the incident flight path for this temporary version was chosen to be 7.5 m rather than the 9 m planned for the final instrument. Otherwise, the temporary version provides a reasonably good simulation of the planned final unit.

Detectors and Position Encoding

The position-sensitive detectors selected are 1.27 cm dia x 60 cm active length ^{3}He-filled gas proportional counters, containing 10 atm of ^{3}He plus

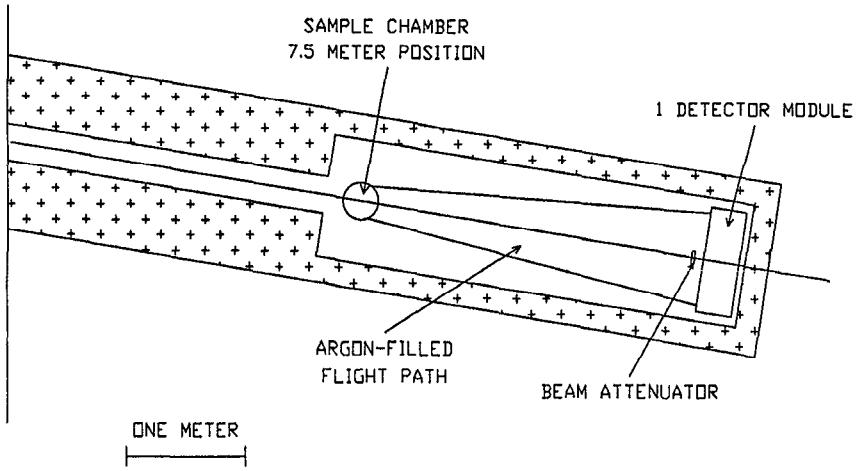

Fig. 4 Temporary GLAD flight path used to gain experience while the flight path shown in Fig. 1 is being fabricated.

additional stopping and quench gases. The resolution specifications require that these detectors be capable of ~ 1 cm resolution along their length, which is compatible with encoding each detector into 64 segments. The intrinsic detector resolution due to the stopping range of the fill gas is ~ 0.5 cm, and the contribution due to the noise in the encoding electronics should be kept to a comparable amount to ensure the desired overall resolution.

The charge-division method is used for position encoding. The neutron detection process starts with the absorption of a neutron at a distance x from end A of the detector. The absorption reaction is

$$n + {}^{3}He \rightarrow {}^{1}H + {}^{3}H + 765\ keV \qquad (1)$$

The resulting proton and triton ionize the stopping-gas molecules, depositing the 765 keV of kinetic energy within a short distance (~ 0.5 cm) of the initial absorption. Gas amplification from the proportional mode operation then leads to a sizable charge being deposited on the anode at position x', which is the projection of the center of the ionization cloud produced by the proton and triton and so may differ from x (by at most ~ 0.5 cm for this fill-gas mixture). If V_A and V_B are respectively the peak voltages output by the charge-sensitive preamplifiers at ends A and B of the detector of length L, then the encoded quantity is

$$\frac{x'}{L} \simeq \frac{V_B}{V_A + V_B} \qquad (2)$$

Data Acquisition Requirements

Based on the final instrument design and the source flux available at IPNS with the new multiplying target, it was estimated that the data acquisition system must meet the following criteria:

Maximum instantaneous data rate per detector	~ 5×10^4 n/sec/det
Maximum time-averaged data rate per detector	~ 1×10^3 n/sec/det
Maximum number of detector elements	~ 450 detectors
64 elements/detector	~ 29,000 elements
Maximum total time-averaged data rate	~ 4.5×10^5 n/sec
Maximum number of time-channels per detector element	~ 1000 channels
Histogram memory per channel	2 or 4 bytes
Maximum histogram memory required with no grouping ~ 29×10^6 channels	~ 60-120 Mbytes

The last result implies that the data acquisition system must group on the average of at least ~ 10 elements per channel on the fly in order to reduce the single-histogram size to a manageable value of ~ 10 Mbytes or less. Strategies for accomplishing this are discussed below.

Data Acquisition

To handle the high instantaneous and time-averaged data rates expected for GLAD, we have developed a new FAST Data Acquisition System (FASTDAS) for use at IPNS. This system is capable of histograming data in a fashion similar to the present microprocessor-based data acquisition systems in use at IPNS, but can build the histograms at a 300 kHz rate and can handle up to 65,536 detector elements. If higher rates prove necessary, multiple FASTDAS systems can be used.

An overview of the system is sketched in Fig. 5, and individual components are shown schematically in Figs. 6-8. This system is made up of Camac digitizer modules (1 for each 4 position-sensitive detectors or 1 for each 8 standard detectors), a special Camac auxiliary-crate-controller module, a custom-designed Histogram Accelerator Multibus board coupled to a Multibus memory array, and a microVax computer also coupled to the Multibus and to a

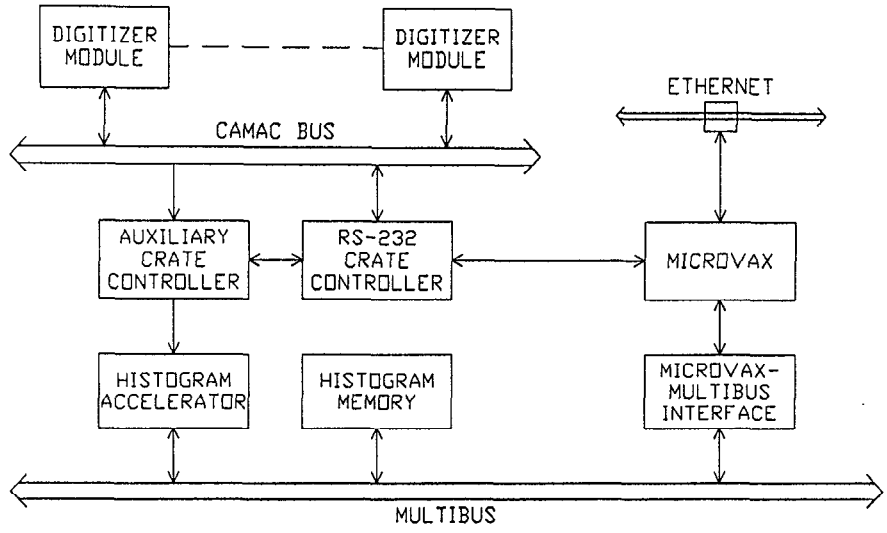

Fig. 5 Block diagram of the GLAD data acquisition system.

Camac crate controller. The microVax computer is also attached to an Ethernet network allowing data files to be sent to other computer systems for analysis.

Camac Digitizer Modules

The Camac digitizer modules (Fig. 6) are custom designed for the particular detectors being used and use a standard Camac interface design. The position-sensitive-detector modules currently in use with FASTDAS can each encode four separate detectors concurrently. "Flash" analog-to-digital converter chips are used to provide rapid encoding. The precision limits of available converters (0.5 bit in 8 bits) result in roughly ± 10 percent variation in the encoded position-channel widths, but this does not pose a serious problem and is accounted for in the calibration process. These modules contain built-in first-in-first-out (FIFO) event buffers with depths of 1024 events, each event made up of 8 bits of detector element ID (encoding 64 positions along each of four detectors) and 16 bits of time information. When an event is stored in the module FIFO the look-at-me (LAM) signal for that module is raised to indicate that that module requires service. The encoding of an event by one of these PSD modules occupies only the detector producing the event and the chain of encoding electronics ("encoding-path") associated with that detector, and requires a deadtime on that encoding-path of 8 μsec. Thus each detector is completely independent as far as deadtime is concerned, and that coupled with this fast encoding means that the system can handle quite high instantaneous

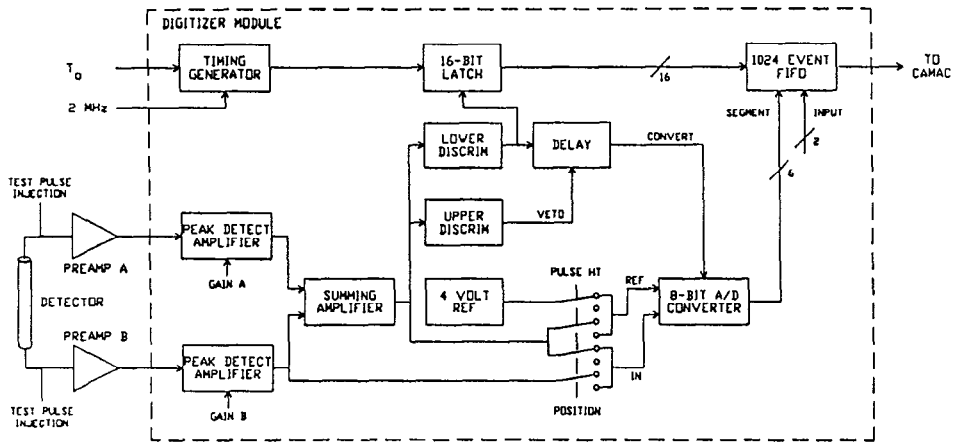

Fig. 6 Schematic representation of the position encoding for one PSD at GLAD, including the detector, preamplifiers, and one of four encoding-paths in a PSD digitizing module. Also shown are the points at which test pulses from pulse generators can be injected for calibration purposes. The digitizer module also provides "offset" and "span" adjustments, but these have been omitted from the drawing for clarity.

data rates without significant deadtime losses. (The projected maximum instantaneous rate per detector of 50000 n/sec/det would lead to deadtime corrections of ~ 40 percent, which is not acceptable. This rate is expected to occur only in rare cases, and then only over a limited time range, but even so, some development efforts will be directed toward reducing this encoding deadtime.)

A useful feature of the PSD digitizing modules is a software-selectable option which allows them to collect data in a 64-channel pulse-height mode for each detector, rather than the usual 64-position mode. This feature greatly facilitates the initial adjustments of the PSD modules and the monitoring of the subsequent performance of individual detectors and encoding-paths (see below).

Camac Auxiliary-Crate-Controller

A specially designed auxiliary-crate-controller module (Fig. 7) has been built to scan the 20 digitizer modules within the crate at a 1 MHz rate. When the controller finds a LAM set it transfers one data word from the digitizer module FIFO to its internal FIFO. This internal FIFO has a depth of 16384 32-bit "events". In addition to the time and element ID from the module, the controller stores the crate and slot number of the module in its FIFO. Thus

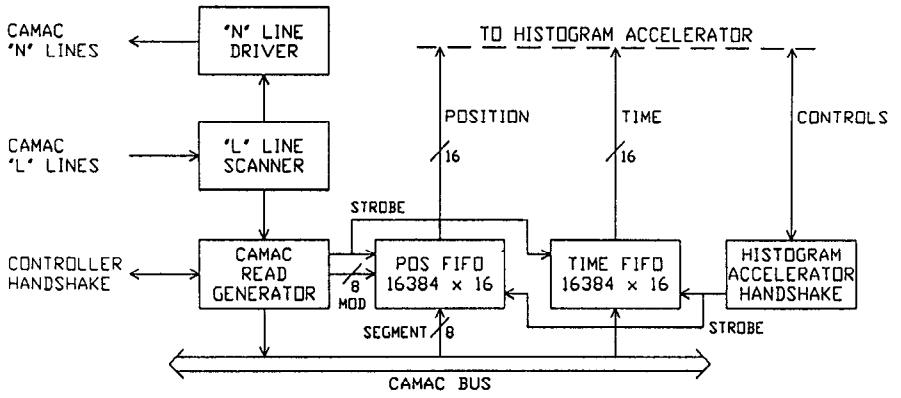

Fig. 7 Block diagram of the Camac auxiliary-crate-controller used with the FASTDAS system.

the controller FIFO contains 16 bits of ID and 16 bits of time for each event. A 32-bit event is supplied from the controller FIFO to the Histogram Accelerator when requested by the latter.

With each module being scanned every 20 μsec the average data rate per Camac module is limited to 50 kHz or 1666 events per IPNS pulse. Since each module contains a 1024-event FIFO the peak data rate per module can be much higher, limited by the module and detector deadtime for a burst of at least 1024 events.

Histogram Accelerator

The FASTDAS Histogram Accelerator (Fig. 8) is a hardware device which contains fast RAM-based lookup tables, adders, and read-increment-write logic for the Multibus memory. This device is implemented on a single Multibus board. All RAM memory on this board is loadable from the microVax computer through the Multibus address space. Using the configuration shown in the block diagram the Histogram Accelerator can duplicate nearly all the features of the software-controlled histograming system presently in operation at IPNS,[2,3] including multiple histograming of each event, rapid switching between histograms for real-time measurements, flexible choice of time channels and detector element grouping, and on-the-fly time focusing. The focusing feature is not currently intended for use with GLAD, but has been designed in so the FASTDAS system can be used on other IPNS instruments as well.

At the start of a histograming cycle, the Histogram Accelerator requests a 32-bit event from the Camac auxiliary-crate-controller FIFO. The 16 bits of

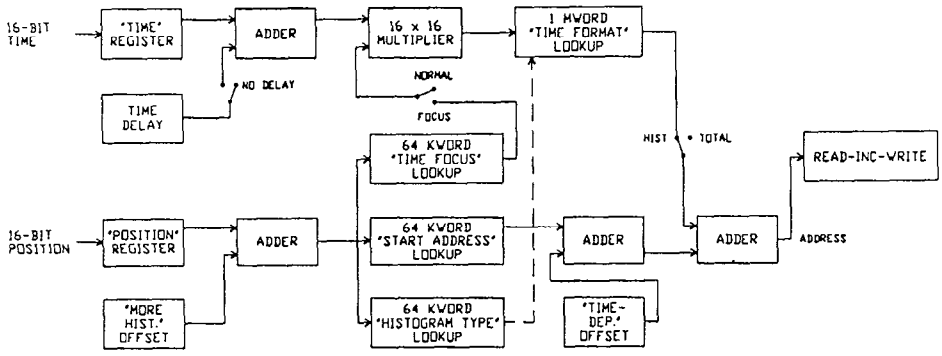

Fig. 8 Block diagram of the FASTDAS Histogram Accelerator. The focus and time-delay options are not intended for use with GLAD, but are included for compatibility with other IPNS instruments.

detector-element ID in this event address a 64 kword lookup table ("start address" table) which contains the "starting address" of the time histogram for that detector element. This "starting address" is the upper 16 bits of a 24-bit address, so each time histogram must start on a 256-byte boundary. The 16 bits of element ID also address a 64 kword lookup table ("histogram type" table) which is used to select different binning algorithms from the time-binning ("time format") table. This histogram type table also contains flags indicating whether data from this ID are to be binned, whether each event from this ID is to be binned in more than one histogram, and whether "on-the-fly time focusing" is to be applied to events from this ID.

The 16 bits of time data first has a constant added to it (contents of the "constant delay" register - set to 0 for GLAD) and, if time-focusing is enabled, is multiplied by a constant obtained from a 64 kword lookup table ("time focus" table) addressed by ID. This result is then used to address a lookup table ("time format" table) which contains the various binning algorithms, using 64 kwords per algorithm with a maximum possible 1 Mwords or 16 algorithms. Each algorithm in this table provides a channel offset number for each 16-bit "modified time value" input to it. A lookup value of zero in this table indicates that the time is out of range and therefore should not be histogramed. This scheme provides complete flexibility in time-binning, permitting conversion of the raw time information to varying numbers of channels per time-histogram and different channel widths at different time values.

If the event is to be histogramed, the address of the 32-bit totalizing counter (which is the time-histogram starting address for this ID), is incremented first. Then the address calculated by adding the channel offset number obtained from the time format table is also incremented. A jumper-

selectable option allows the histograming to occur in either 16-bit channels or in 32-bit channels. In the 16-bit case, any overflows which occur because of these increments will be recorded in a FIFO (not yet implemented), and attached to the data set when it is read out by the microVax.

Once the Histogram Accelerator has completed all required histograming for this event it immediately requests another event from the auxiliary-crate-controller FIFO, so the Histogram Accelerator is the controlling factor in the overall histograming rate. The table lookups and memory incrementing are limited mainly by the Multibus access time and the memory cycle time of the Multibus memory used. With the current 400 nS cycle time memories, a time-averaged histograming rate of over 300 kHz has been measured. This is already close to the estimated maximum rate of 450 kHz for GLAD, and so should be adequate for some time to come. (Two such systems could be used to double the histograming rate if necessary.) The Histogram Accelerator has the capability of multiplexing data from eight Camac auxiliary-crate-controllers, thus allowing for a total of 160 digitizing modules (640 linear PSDs) in a system.

Multibus System

The Multibus system is of the same type as is currently used in the other IPNS data acquisition systems.[2,3] The Multibus has 24 memory address lines which allows for the addressing of up to 16 Mbytes of memory (1 "Mbyte" is really 2^{20} or 1,048,576 bytes). Of this 16 Mbytes, 1.5 Mbytes are needed to address the Histogram Accelerator lookup tables (nearly 3 Mbytes are used for these tables, but since word-addressing is used on the Histogram Accelerator board this requires only 1.5 Mbytes of Multibus "address space"), thereby leaving 14.5 Mbytes available for histogram data. Multibus memory, including the lookup tables on the Histogram Accelerator board, is accessible by the microVax-to-Multibus interface which can address all 24 bits of address space. This interface is nearly the same as that currently used with the PDP computers on the other IPNS instruments,[2] requiring only minor switch-selectable modifications. However, the software driver for this interface had to be modified for use on a microVax.

MicroVax-to-Camac Interface

Unlike the microprocessor-based system used on other IPNS instruments, the FASTDAS Histogram Accelerator issues no commands to the Camac system. Instead, a microVax-to-Camac interface has been included to provide the capability to initialize Camac modules and control data acquisition directly from the microVax. Since there are no speed dependent functions which must occur via

this link, this interface is via an RS-232 Camac crate controller for simplicity.

PSD Adjustment, Calibration, and Monitoring

With such a large number of detectors, an efficient calibration procedure and the associated hardware and software features to facilitate calibration and to ensure the reliability of this calibration are very important. In developing these, we have benefited considerably from the previous experience with PSDs at the University of Missouri[4] and at IPNS.

A number of hardware features intended to aid in PSD adjustment, calibration, and monitoring have been incorporated into the GLAD system from the outset. Two of these, the position calibration mechanism which is an integral part of each detector module and the pulse-height data acquisition mode for the PSD digitizer modules, have already been noted above. In addition, separate power supplies have been provided for the upper (A) and lower (B) banks of preamplifiers, allowing either bank to be turned on or off independently and remotely; test-pulse input points are connected to each A and B preamplifier; and programmable tail-pulse generators allow independent injection of test pulses of known amplitudes into either the A or B (or both) banks of preamplifiers. The procedures for PSD adjustment, calibration, and monitoring based on these hardware capabilities (and correspondingly developed software) are outlined briefly below. With all these features in place, the operation and maintenance of the ~ 450 detectors encoded into ~ 29,000 position elements should be relatively painless and quite reliable.

Initial Adjustment Procedure for Camac PSD Digitizing Modules

This procedure must be carried out whenever a new detector, preamplifier, or PSD digitizing module is installed, but need be repeated only infrequently otherwise. These steps can be followed concurrently for any number of detectors. First the gains must be set and balanced for the A and B signals for each detector. This is done with the detectors illuminated with neutrons from a strongly scattering sample placed in the beam or from a PuBe source placed in the sample position or near the detectors. First, only the A preamplifiers are powered, the PSD modules are operated in pulse-height mode, and the gain of each input is adjusted to give the desired pulse-height spectrum. The same is then done with only the B preamplifiers powered. Next, both A and B preamplifiers are powered with the PSD module still in pulse-height mode, and the lower discriminator levels are adjusted to cut off the

pulse height spectra at the desired level (upper discriminator levels are not adjustable). An example of such pulse height data at this stage is shown in Fig. 9. Finally, the PSD modules are switched to position mode and position spectra are acquired with the absorbing bar in two different locations (~1/4 and ~3/4 of the detector length) between the neutron source and the detectors. This last step is repeated while adjusting the "Offset" and "Span" controls on the PSD modules until the bar shows up in the same position channels on all detectors. Figure 10 shows such position calibration data for several detectors for one position of the absorbing bar. These data were collected before the final "Offset" and "Span" adjustments had been completed, so some unused channels occur at each end of the range and the absorbing bar does not appear at quite the same channels for each detector.

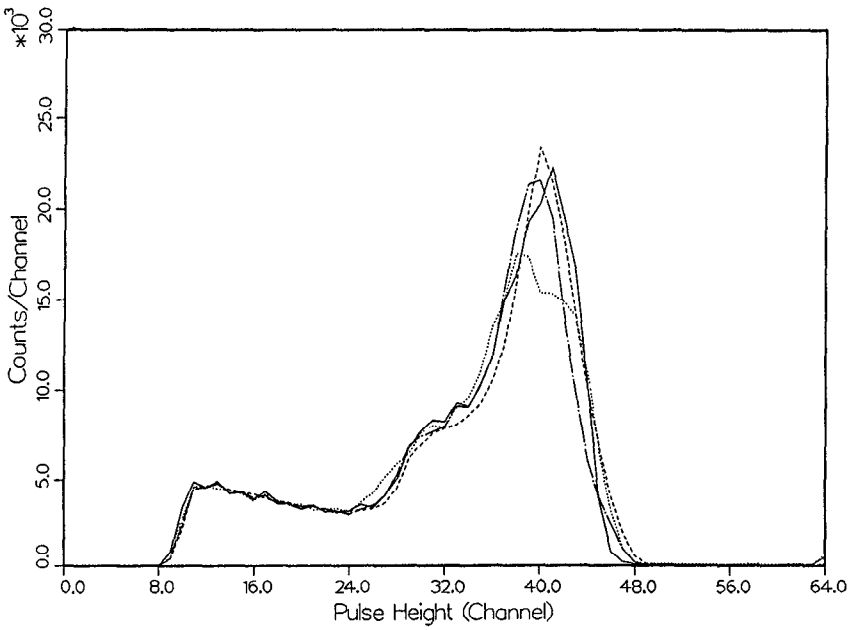

Fig. 9 Pulse-height data simultaneously collected from four different detectors, using a PuBe neutron source, after the initial PSD adjustments have been performed. These variations among detectors are typical.

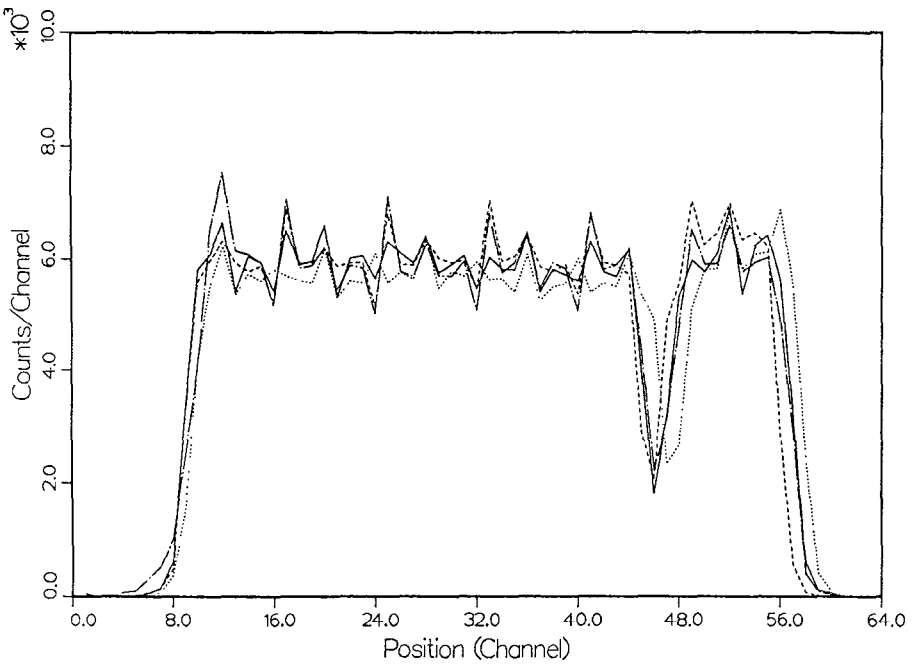

Fig. 10 Position data simultaneously collected from four different detectors, using a PuBe neutron source, after the initial PSD adjustments have been performed but before the final "Offset" and "Span" adjustments have been completed. The absorbing bar was positioned in front of the detectors, and its shadow is seen to be in nearly the same position on all four detectors even though the adjustments were not yet complete. The variation of intensity with channel for channels away from the bar position is due to irregularities in channel widths introduced by the limited precision of the analog-to-digital converters.

Determination of the Absolute Channel-to-Position Mapping

This needs to be done after the initial adjustment, and repeated only occasionally as a check against drifts. This procedure requires a smoothly-varying known distribution of neutrons (a uniform distribution is best), which can again be provided by a strongly scattering sample in the beam or by a PuBe source at the sample position. It is necessary to record position spectra in all detectors with the absorbing bar in several different known positions. These data are fit to determine the detector resolution and the positions corresponding to the boundaries of each position channel for each detector. These results are then stored in an instrument calibration file, for subsequent use by the data analysis routines as noted below.

Automatic Monitoring of Calibration Drifts

No neutrons are needed for this. Before the automatic monitoring can be implemented, it is first necessary to provide an information base for this purpose. This can be generated with only a minimum of manual intervention, and should be done immediately following the initial adjustment procedure. The first item in this information base is a record of all the individual encoding-path gains (each end of each detector). This is obtained by powering each preamplifier bank (A or B), one at a time, injecting test pulses of known magnitude, and recording the pulse-height channels which accumulate these pulses for each detector. The second item is a record of discriminator settings for each detector. To obtain this, both preamplifier banks are powered, test pulses spanning a range of amplitudes are injected into one preamplifier bank, and for each detector the lowest test-pulse amplitude which is accumulated is recorded. The third and final item is an indication of the relative position mapping for each detector. This is obtained by powering both preamplifier banks, injecting test pulses of different known amplitudes into banks A and B, and recording for each detector the position channels into which these events are accumulated. This provides a record of the overall position mapping.

Once this information base is available, it can be used to test automatically all the detectors and encoding electronics to ensure that no drifts have occurred since the initial calibration. The basic test is a repeat measurement of the relative position mapping data (the third set of measurements in the information base), comparing the results with the values recorded in the information base for each detector. If further information is desired, either or both of the first two sets of measurements in the information base can be repeated and the results compared with the values previously recorded. All of this can be done automatically in a relatively short time with no user intervention, and so can be included as part of a standard startup procedure at the start of each run or other suitable interval. If any values have shifted by more than the allowed limits, the user can be warned and any other desired action (such as refusing to start the run) can be taken.

Data Handling and Analysis

Data Collection Strategies

The philosophy for the initial data analysis assumes elastic scattering, i.e., $k_1 = k_0 = 2\pi/\lambda$. Inelasticity effects are considered as a correction to

be made later. We consider two types of sample. The simpler case is an isotropic sample, for which data are required only as a function of the scalar variable.

$$Q = \frac{4\pi}{\lambda} \sin \theta \tag{3}$$

where 2θ is the scattering angle between incident and scattered wavevectors. The more complicated case is that of a full three-dimensional structure, e.g., of a single crystal or of a bulk glass or film with orientational effects. In this case the data are required as a function of the vector variable

$$Q = \frac{2\pi}{\lambda} (1 - \cos \psi \cos \phi, - \cos \psi \sin \phi, - \sin \psi) \tag{4}$$

where ψ and ϕ are polar coordinates of a detector element (see Fig. 11). These are related to θ by

$$\cos 2\theta = \cos \psi \cos \phi \, . \tag{5}$$

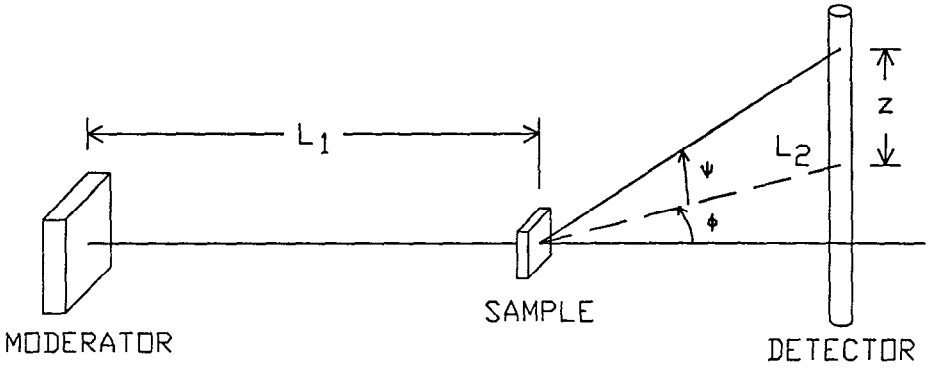

Fig. 11 Geometry for data analysis.

The data must be histogramed so as to meet the requirements that (a) the size of the data sets is manageable, (b) the channel widths in both time and angle do not make a significant contribution to the experimental resolution, and (c) the outcome of the experiment should be as insensitive as possible to failure of single components. As is usually the case, these requirements are not strictly compatible: (b) and (c) would dictate that each vertical element in each detector is binned into a separate time histogram, but as noted earlier this requires on the order of 60 Mbytes per measurement, which exceeds the available memory on the present system and in any case would be unmanageably large. Some compression of the data must therefore be made on line in order to stay within the memory limits and also to keep the data sets to a reasonable

size. For example, it would be convenient to be able to store onto a single magnetic tape the output from a series of, say, eight samples inserted into an automatically cycling sample changer, which implies a maximum of around 15 Mbytes per sample; and even smaller sets would further simplify the tasks of data transfer, analysis, and archiving.

For the case of isotropic samples, the obvious way to compress the data at collection time is to bin the detector elements into a histogram of scattering angle $2\theta \pm \Delta\theta$, with events from all elements lying within this angular range being binned in a single time histogram. The bin width $2\Delta\theta$ will then introduce a contribution of $0.68\ \Delta\theta \cot\theta$ into the FWHM $\Delta Q/Q$ resolution. Choosing these bin widths to make this contribution somewhat smaller than the calculated $\Delta Q/Q$ resolution due to other geometrical effects in the present design requires ~ 315 2θ channels to cover the entire angular range (0.3° to 90°).

Actually, this mode of histograming provides more compression than would be required initially at data collection time. Thus it is proposed that during the data collection the elements contributing to a given 2θ bin be grouped with a separate time histogram for each set of such elements arising from the same detector (or small subset of the detectors). Advantages of this are: (a) deadtime corrections can be readily applied since, in a given detector, these depend on the count rate up to that time over all elements in the detector; (b) a faulty detector may be dropped without jeopardizing the whole 2θ bin; (c) the variation in flight path length is greatly reduced if only elements in a single detector are involved, so this contribution to the resolution is minimized; and (d) the same conceptual scheme (but with different grouping to provide the desired coverage of ϕ,ψ space defined in Fig. 11) may be used for anisotropic samples.

Calibration Procedure

For a neutron travelling a total path length L and detected at time t from its point of origin, the wavelength can in principle be determined from

$$\lambda = \frac{ht}{mL} . \qquad (6)$$

In practice, the neutron production and moderation processes make it impossible to determine t and L absolutely. Ikeda and Carpenter[5] developed detailed descriptions of the time distributions of neutron emission from the moderator. In the Ikeda-Carpenter description the emission time t_e, which is the delay between the time origin (the "t_o pulse" at IPNS) and the mean of the time distribution for emission of neutrons of wavelength λ, can be written as

$$t_e = t_o + 3m\lambda/h\Sigma(\lambda) + \exp(-\lambda_o^2/\lambda^2)/\beta \tag{7}$$

where t_o is a fixed time-triggering offset, $\Sigma(\lambda) = (s_1 + s_2\lambda^2)^{1/2}$, $\lambda_o = (h^2/2mE_o)^{1/2}$, and s_1, s_2, E_o and β are constants defined by Ikeda and Carpenter and subject to measurement for a particular moderator. For a neutron recorded in a time channel centered at a time t' relative to the time origin, Eq. (6) must thus be replaced by

$$\lambda = h\,\frac{[t' - t_o - 3m\lambda/h\Sigma(\lambda) - \exp(-\lambda_o^2/\lambda^2)/\beta]}{mL} \tag{8}$$

(or by a corresponding equation if a different formulation is used to represent the emission-time delay).

Sinclair, Tasker, Clare, and Wright[6] describe the procedure for determining L and t_o for a given detector element. This procedure involves the careful measurement of powder diffraction patterns from known samples as well as the use of a series of sharp wavelength markers, such as resonant absorbers, single-crystal Bragg reflections, or polycrystal Bragg edges, in the incident beam. The GLAD incident beamline will include provision for easy insertion of such filters for calibration.

In determining the angle ψ for each detector element, the absorbing bar calibration procedure described above is used to obtain values $z(\ell,m)$ for the height (above or below the instrument midplane) of each element (m) in each detector (ℓ). The angle $\psi(\ell,m)$ is then given by

$$\psi(\ell,m) = \tan^{-1}\left(\frac{z(\ell,m)}{L_2(\ell)}\right) \tag{9}$$

where $L_2(\ell)$ is the distance from sample center to the center of the ℓ^{th} detector on the instrument midplane, which is determined by measurement after construction of the flightpath. The value of $L(\ell,m)$ is then obtained from

$$L(\ell,m) = [L_1 + L_2(\ell)] + [L_2^2(\ell) + z^2(\ell,m)]^{1/2} - L_2(\ell) \tag{10}$$

The set of quantities $\{t_o, s_1, s_2, E_o, \beta, \phi(\ell), L(\ell,m), \psi(\ell,m)\}$ will be stored on the microVax as the basic calibration file for the instrument. It should be updated periodically to allow for changes in detector calibration, changes in moderator properties, changes in geometry due to shifts in the floor, and other factors which alter with time.

Data Analysis

In a given run, an intensity histogram $I(\ell,k,n)$ is measured as a function of detector (ℓ), angle group (k), and time channel (n). Each $I(\ell,k,n)$ will be affected by deadtime, the effect being related to the count rate in the preceeding time channels summed over all elements for that detector. Since the deadtime will have a fixed value (8 μsec) which has been set in the electronics design, the effect can be calculated to give a deadtime-corrected histogram $I_c(\ell,k,n)$. The wavelength $\lambda(\ell,m,n)$ associated with each time channel for each detector element can be determined by iteratively solving Eq. (8) for a given time-histogram setup. These results can then be averaged to provide an average wavelength $\lambda(\ell,k,n)$ for each detector, angle group, and time-channel combination. A typical experiment includes a number of runs measuring samples, backgrounds, empty containers, and vanadium for normalization, leading to a "primary" data set consisting of

$$S_1 = \{I_{c1}(\ell,k,n),\ldots,I_{cp}(\ell,k,n),\lambda(\ell,k,n),\Theta(\ell,k),\psi(\ell,k)\} \tag{11}$$

where the indices 1...p extend over all the runs in this experiment.

For isotropic samples, it is not necessary to retain the identity of the detector, so the histograms can be summed over ℓ to give $I_c(k,n)$; similarly, the $\Theta(k)$ and $\lambda(k,n)$ can be obtained by appropriate averaging. The "secondary" data set for isotropic samples can then be taken as

$$S_2 = \{I_{c1}(k,n),\ldots,I_{cp}(k,n),\lambda(k,n),\Theta(k)\} \tag{12}$$

This can be expected to be the level at which most users will transfer their data.

In the final stage of analysis, all the remaining corrections must be considered, including multiple scattering, absorption, background and container partially debugged, and hope to begin commissioning of this instrument in earnest at that time. We have also received the soller collimators (Cidic, Ltd., Cheltenham, England) and hope to install them, along with some additional incident beamline components, later this fall. We will then be able to test essentially the complete incident beamline (excluding choppers) to be used on the final version of the instrument.

The design is nearly complete for the final version of the GLAD scattered flight path. We hope to have this flight path built, and to provide enough detectors and electronics for two more detector modules to go with this path, during the coming year. At the same time, we are beginning to develop the

ancillary devices, such as cryogenic and high-temperature environments with sample changers, necessary for the performance of quality science at such an instrument. Thus by the end of 1989 the final version of GLAD should be in place with a complement of ~160 detectors, and should be beginning commissioning. This detector complement should be adequate for many of the envisioned scientific problems, and we expect scientific research on GLAD to begin on a routine basis in 1990, although the choppers for elastic scattering studies may not yet be in place at that time. Additional detectors will be added as funding permits until the full complement of ~450 detectors is reached.

The data acquisition system is close to meeting the design goals set forth earlier in this paper, but several additional development steps remain to bring the final instrument up to its ultimate level of performance. New preamplifiers must be developed to improve the PSD position resolution while retaining or increasing the encoding speed. The present resolution is ~ 1.6 cm FWHM, while a resolution of ~ 1 cm is desired. We would also like to develop faster encoding (preamplifiers and/or digitizing modules) to reduce the deadtime below the present 8 μsec per event per detector, to reduce deadtime losses to acceptable levels at the estimated maximum instantaneous data rates. The 300 kHz histograming speed is already adequate for all but the most demanding situations anticipated, but may need to be increased somewhat by the time the full complement of detectors is installed. It would be desirable to develop software techniques to reduce the time required to calculate and download the histograming tables and start a run, since with the present software this can be several minutes per time-binning table if many channels scattering, and Placzek corrections. These depend on both λ and Θ. Routines used at this stage will be similar to those currently in use for glass data from SEPD and GPPD at IPNS. The final data set for isotropic samples then has the form

$$S_3 = \{I_1(j),\ldots,I_p(j),Q(j)\} \ . \qquad (13)$$

where the index j runs over all the Q bins used in this analysis.

Status and Results

The temporary flightpath for GLAD was installed in May, 1988, allowing data collection for ~ 2 weeks before the summer shutdown of IPNS (only 12 of the 55 detectors were in place for this period). During this running period we were able to perform the initial PSD adjustments (see above and data in Figs. 9-10) and to verify that the FASTDAS system, the position and time encoding of the

the PSDs, and the basic microVax data acquisition software all worked satisfactorily. We also confirmed that the PSDs could be operated satisfactorily in line with the direct beam, with the beam being attenuated only by a 2.5 cm thick B_4C/epoxy "beam attenuator" directly in front of the detectors. Detector recovery problems were apparent at times shorter than 500 μs after the prompt pulse, but recovery was nearly complete by 500 μs (which is the time-of-flight for 0.19 Å neutrons). Figure 12 shows time-of-flight data from the individual segments for the detector centered on the beam. These data were collected while there was still a significant amount of air in the scattered flight path, and so show a strong air-scattering background reflecting the spectral shape of the incident spectrum. The shadow of the beam attenuator is clearly evident in this figure.

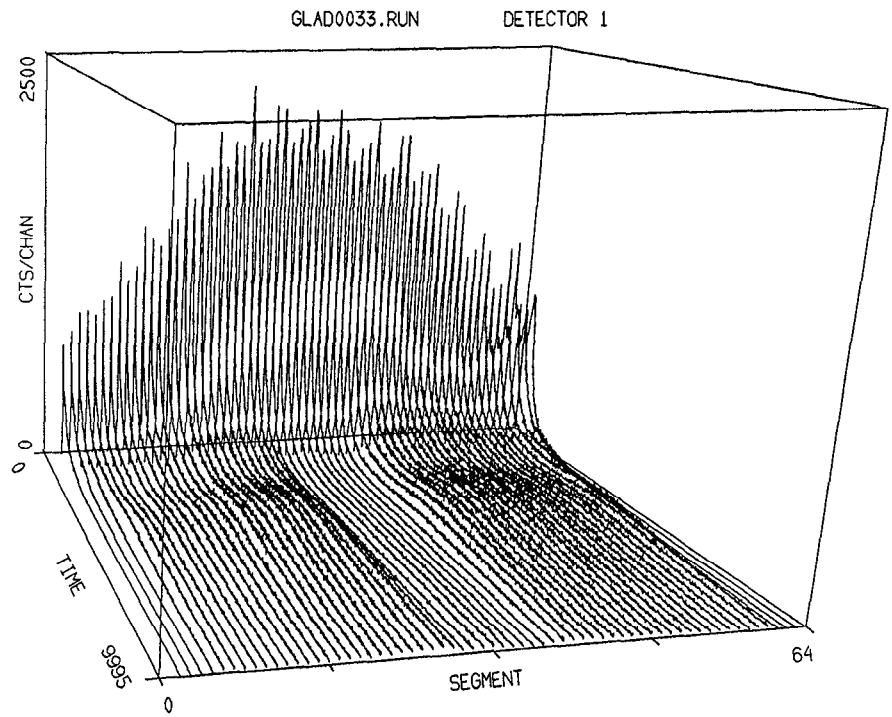

Fig. 12 Example of initial time-of-flight data from a single detector (64-segments) with the GLAD temporary flight path. A strong background at short times is seen, while the spectral features at longer times are primarily due to neutrons scattered from residual air in the flight path, and reflect the incident neutron spectrum. This detector was centered on the neutron beam, with the beam being attenuated only by the "beam attenuator". No adverse affects from this beam loading are seen at times > 500 μs, but the beam attenuator is clearly seen as a shadow in the air-background scattering.

The limited amount of running time did not permit a thorough background study, but did pinpoint a number of potential problems. Several shielding modifications were made during the summer, which should reduce the background from some of these sources. During the summer, we also installed the additional detectors and electronics to bring the single detector module up to its full complement of 55 detectors. Thus we will to begin the Fall, 1988, running period with the temporary instrument version fully assembled and and a long time range are used. We would also like to reduce the time required to save data to a file, since this can be significant for the large data sets contemplated. Because of the size of the run files, we will also need to develop new techniques for archiving of run files and/or partially reduced $I(\theta,\lambda)$ data. We expect that most of these problems will be solved by the time the final flight path is installed.

A significant remaining problem is background, particularly the background at short times which is so evident in Fig. 12. Much of the running time with the temporary flight path is expected to be devoted to the development of effective techniques for background reduction.

Acknowledgments

The authors would like to thank D. Bohringer and R. Stefiuk for their work on the design of the temporary GLAD flight paths and M. Faber for his work with the GLAD detector systems. A large number of people from the IPNS operations and accelerator groups were involved in the construction of the temporary GLAD instrument and the fabrication of the detector electronics, and we gratefully acknowledge these efforts. Discussions with R. Berliner and D. F. R. Mildner at the University of Missouri were very helpful in the initial design of the position-sensitive-detection electronics and the position-calibration procedures. This work was supported by the U.S. Department of Energy, BES, contract No. W-31-109-ENG-38.

References

1. A. C. Nunes, Nucl. Instrum. Methods, 119, 291-293 (1974).
2. J. R. Haumann, R. T. Daly, T. G. Worlton, and R. K. Crawford, IEEE Trans. Nucl. Sci., NS-29, 62-66 (1982.
3. J. R. Haumann and R. K. Crawford, IEEE Trans. Nucl. Sci., NS-34, 984-953 (1987).
4. R. Berliner, D. F. R. Mildner, O. A. Pringle, and J. S. King, Nucl. Instrum. Methods, 185, 481-495 (1981).
5. S. Ikeda and J. M. Carpenter, Nucl. Instrum. Methods, A239, 536-544 (1985).
6. R. N. Sinclair, C. G. Tasker, A. G. Clare, and A. C. Wright, Nucl. Instrum. Methods, A240, 199-202 (1985).